CORE
Metadata, citation and similar papers at core.ac.uk
Provided by Copenhagen University Research Information System

UNIVERSITY OF COPENHAGEN

Observation and spectroscopy of a two-electron Wigner molecule in an ultraclean carbon nanotube

Pecker, S.; Kuemmeth, Ferdinand; Secchi, A.; Rontani, M.; Ralph, D.C.; McEuen, P.L.; Ilani, S.

Published in:
Nature Physics

DOI:
10.1038/nphys2692

Publication date:
2013

Document version
Publisher's PDF, also known as Version of record

Citation for published version (APA):
Pecker, S., Kuemmeth, F., Secchi, A., Rontani, M., Ralph, D. C., McEuen, P. L., & Ilani, S. (2013). Observation and spectroscopy of a two-electron Wigner molecule in an ultraclean carbon nanotube. *Nature Physics*, *9*, 576-581. https://doi.org/10.1038/nphys2692

Download date: 08. Apr. 2020

ARTICLES
PUBLISHED ONLINE: 28 JULY 2013 | DOI: 10.1038/NPHYS2692
nature physics

Observation and spectroscopy of a two-electron Wigner molecule in an ultraclean carbon nanotube

S. Pecker[1†], F. Kuemmeth[2†], A. Secchi[3,4‡], M. Rontani[3], D. C. Ralph[5,6], P. L. McEuen[5,6] and S. Ilani[1*]

Two electrons on a string form a simple model system where Coulomb interactions are expected to play an interesting role. In the presence of strong interactions, these electrons are predicted to form a Wigner molecule, separating to the ends of the string. This spatial structure is believed to be clearly imprinted on the energy spectrum, yet so far a direct measurement of such a spectrum in a controllable one-dimensional setting is still missing. Here we use an ultraclean carbon nanotube to realize this system in a tunable potential. Using tunnelling spectroscopy we measure the addition spectra of two interacting carriers, electrons or holes, and identify seven low-energy states characterized by their exchange symmetries. The formation of a Wigner molecule is evident from a tenfold quenching of the fundamental excitation energy as compared with the non-interacting value. Our ability to tune the two-carrier state in space and to study it for both electrons and holes provides an unambiguous demonstration of this strongly interacting quantum ground state.

One of the simplest realizations of an interacting quantum-mechanical system is that of two electrons on a string. The behavior of this system is governed by the balance between kinetic and interaction energies. When kinetic energy dominates, the electrons occupy particle-in-a-box levels along the string. In contrast, when interactions dominate, a Wigner-molecule ground state is formed, in which the repulsion of the two electrons drives them to localize at the two sides of the string[1,2]. Owing to the fermionic nature of the two particles their total wavefunction is anti-symmetric with respect to electron exchange, leading to an intimate connection between their real-space and spin-space behaviours. Consequently, the real-space charge separation in a Wigner molecule goes hand in hand with a spin-space signature, namely a pronounced quenching of its spin excitation energies[3].

A carbon nanotube is an excellent system to search for the existence of a Wigner-molecule ground state. This system is known to have strong electron–electron interactions[4–8], and can be clean enough to allow measurements down to the single-carrier limit[9,10], made more accessible by recent technological breakthroughs[11–14]. Some of these measurements showed unexplained deviations from the expected shell-filling model, which hinted that interesting physics occur at low electronic numbers[9,11,12]. Compared with III–V semiconductor systems[15–18] in which Wigner-molecule formation has been explored previously, in suspended nanotubes the screening of Coulomb interactions is strongly reduced and the one-dimensional confinement potential for electrons or holes can be shaped with gate electrodes. This ability to control the confining potential is critical because it allows one to distinguish between extrinsic electrostatic effects that spatially separate the two electrons and intrinsic separation driven by their repulsion. Furthermore, in addition to the conventional twofold spin degeneracy in other semiconductors, electrons in nanotubes possess a twofold orbital degeneracy (isospin), forming a fourfold spin–isospin subspace. Recent experiments[12] have shown that the electrons' spin and isospin in nanotubes are easily polarized by magnetic fields, which has been interpreted as an indication of Wigner-crystal order. However, more recently single-particle spin–orbit coupling has been found in this system[13,19,20], which can also preferentially align the spins and isospins in a way similar to electron–electron interactions. In an attempt to unambiguously identify the effects of interactions, recent theoretical works have focused on the case of two electrons, and have demonstrated that the role of interactions can be directly determined by measuring the excitation spectrum[21–25]. Two-electron excitations also play a key role in making quantum bits in nanotubes[26]. However, because interactions may hinder qubit implementation by suppressing Pauli-blockade physics[14,21,25], experiments so far have been performed in the non-interacting regime (due to geometry, dielectric environment and level spacing)[20,27–30]. A measurement of the excitation spectrum of two electrons in the opposite regime of strong interactions has so far been missing, and holds the key for determining the strongly interacting nature of this system.

In this work we probe the addition spectrum of two carriers, electrons or holes, confined to a nanotube quantum dot by transport spectroscopy. We present data obtained from a single device that had especially low disorder. We identify seven low-energy quantum states that fall into two multiplets that are symmetric or antisymmetric under particle exchange in real space. We find that a single-particle description of the two-electron system with spin–orbit coupling captures well the addition spectrum within each multiplet. Interestingly, however, the energy splitting between the two multiplets is quenched by an order of magnitude compared with its non-interacting value. We show that this quenching is a direct manifestation of the formation of a Wigner-molecule state. We demonstrate the generality of our observation and the absence of disorder by measuring similar spectra for electrons and holes in the same device, having opposite response to disorder potential.

[1]Department of Condensed Matter Physics, Weizmann Institute of Science, Rehovot 76100, Israel, [2]Center for Quantum Devices, Niels Bohr Institute, University of Copenhagen, Universitetsparken 5, DK-2100 Copenhagen, Denmark, [3]CNR-NANO Research Center S3, Via Campi 213/a, 41125 Modena, Italy, [4]Department of Physics, University of Modena and Reggio Emilia, 41125 Modena, Italy, [5]Physics Department, Cornell University, Ithaca, New York 14853, USA, [6]Kavli Institute at Cornell, Cornell University, Ithaca, New York 14853, USA. †These authors contributed equally to this work. ‡Present address: Institute for Molecules and Materials, Radboud University of Nijmegen, 6525 AJ Nijmegen, The Netherlands. *e-mail: shahal.ilani@weizmann.ac.il

© 2013 Macmillan Publishers Limited. All rights reserved

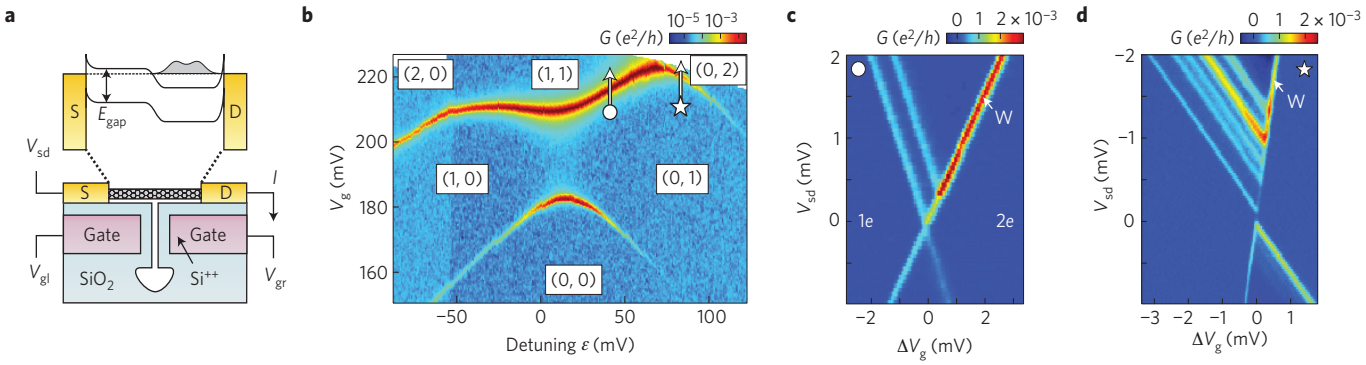

Figure 1 | Addition energy spectra of a two-electron molecular state in an ultraclean nanotube. a, Device schematic. A single ultraclean nanotube is contacted by source (S) and drain (D) electrodes separated by 500 nm and suspended over two gate electrodes. The two gates induce a controllable electrostatic potential along the tube, as depicted by the energy band diagram. **b**, Measured charge stability diagram of the device. The differential conductance of the device, $G = \mathrm{d}I/\mathrm{d}V_{sd}$ (where I is the current and V_{sd} is the source–drain bias), is plotted as a function of common voltage $V_g = (V_{gr} + 2.4V_{gl})/3.4$ and detuning $\epsilon = (V_{gr} - V_{gl})/3.4$ (V_{gr} and V_{gl} are the right and left gate voltages). Index pairs (n,m) denote the charge configuration, where n (m) is the number of electrons on the left (right) side of the nanotube. **c**, Conductance through the nanotube measured as a function of V_g and V_{sd}, around the transition between (0,1) and (1,1) configurations (circle in **b**). The conductance exhibits a sharp peak whenever the electrochemical potential in one of the leads equals the energy difference between 1e and 2e states. The two parallel lines on the top left then correspond to the 2e states and the one on the right, marked W, corresponds to the edge of the spectroscopic window. **d**, Similar measurement around the transition between (0,1) and (0,2) configurations (star in **b**). More 2e states are observed in this case as compared with **c**. The visibility of excited 2e states depends on bias direction due to asymmetric tunnel coupling to the leads (Supplementary Section S6).

Our device, used previously to study spin–orbit coupling of one electron ($1e$) in a single quantum dot, is now used to study two-electron ($2e$) states in a molecular regime. We obtain essentially identical results for two holes (Supplementary Section S5). The device consists of a nanotube suspended above a pair of split-gate electrodes and contacted by source and drain electrodes (Fig. 1a). The charge stability diagram, measured as a function of the common voltage on the gates, V_g, and their difference (detuning), ϵ, (Fig. 1b) shows a rounded honeycomb structure, similar to that of a strongly tunnel-coupled double dot. This molecular configuration allows us to continuously transform between two different $2e$ configurations: in one, the electrons are localized in different sites near the two ends of the nanotube (the $(1,1)$ configuration), whereas in the other, both electrons occupy the same site (the $(0,2)$ configuration). Figure 1c,d shows the measurement of the $2e$ addition spectra in these two configurations. For each configuration we measure the differential conductance, $G = \mathrm{d}I/\mathrm{d}V_{sd}$, as a function of source–drain bias, V_{sd}, and V_g. The parallel lines observed within these Coulomb diamonds correspond to the individual $2e$ excited states. Below we will show that the different spectra, observed in these two configurations that differ by the detuning, provide crucial information for understanding the role of interactions in these molecular states.

The interacting nature of two-electron states is expected to be clearly imprinted on their detuning-dependent addition spectrum, shown schematically for the non-interacting case in Fig. 2a, and for the strongly interacting Wigner-molecule case in Fig. 2b. On the left side of the figure (low detuning) the two electrons are in the $(1,1)$ molecular configuration, separated to the two sides of the nanotube. On the right side, the two electrons are in the $(0,2)$ molecular configuration, both occupying the same side. As detuning increases the energy of the left side with respect to that of the right side, each state in the $(1,1)$ configuration rises in energy, whereas each state in the $(0,2)$ configuration falls in energy. In the figure we colour the $2e$ states according to their symmetry with respect to electron exchange in real space: the ground state is always symmetric in real space (red) whereas the first excited state is anti-symmetric in real space (blue). In the non-interacting limit and when the two electrons are on the same side (right side of Fig. 2a) in a spatially symmetric $2e$ wavefunction the two electrons can both occupy the lowest particle-in-a-box level, whereas in a spatially antisymmetric wavefunction one electron must occupy the next particle-in-a-box level. Thus, in the non-interacting limit there is a large symmetric–antisymmetric splitting, Δ_{S-AS}, equal to the single-particle level spacing, Δ_{ls}. The situation is very different in the presence of strong interactions (Fig. 2b), which drive the two electrons apart in real space. Such electronic separation has very little effect on the antisymmetric state, where the electrons are already separated in real space by virtue of symmetry, but it has a marked effect on the symmetric ground state, in which in the absence of interactions both electrons strongly overlap. Interactions drive the density profile of the symmetric and antisymmetric states to be essentially identical (Fig. 2b), and correspondingly, their energy splitting becomes strongly suppressed, $\Delta_{S-AS} \ll \Delta_{ls}$. The symmetric–antisymmetric splitting, Δ_{S-AS}, thus serves as a quantitative measure of the interaction strength and the real-space separation of a Wigner molecule.

The same reasoning holds regardless of whether the two electrons occupy the $(1,1)$ or $(0,2)$ configuration. In fact, in the $(1,1)$ case the suppression of Δ_{S-AS} should be even more pronounced than for the $(0,2)$ case. As will be shown below we indeed measure, as in previous works[15,18], suppressed Δ_{S-AS} for the $(1,1)$ configuration. We note, however, that in the $(1,1)$ configuration each electron is near an edge, and as such it is inherently attracted to its image charge in the metallic contact and the gate on one side of the nanotube. This attraction creates an effective single-particle double-dot potential along the entire suspended length of the nanotube. When two electrons occupy such an effective single-particle potential, even weak interactions would lead to the formation of an artificial Wigner molecule, where each electron sits in a dot. In this case, the separation between the electrons is not determined by the interactions, but simply by the distance between the dots. To critically test the effect of interactions between the electrons we must therefore localize them near one edge, effectively in a single dot. Sitting in a single-dot confinement potential, their separation is determined by their mutual repulsion. The ability to squeeze the electrons to one side of the tube, used in this work, is thus fundamental for pinpointing the effects of their mutual repulsion.

To adapt the above picture to a nanotube we need to recall that for each particle-in-a-box state along the nanotube there

© 2013 Macmillan Publishers Limited. All rights reserved

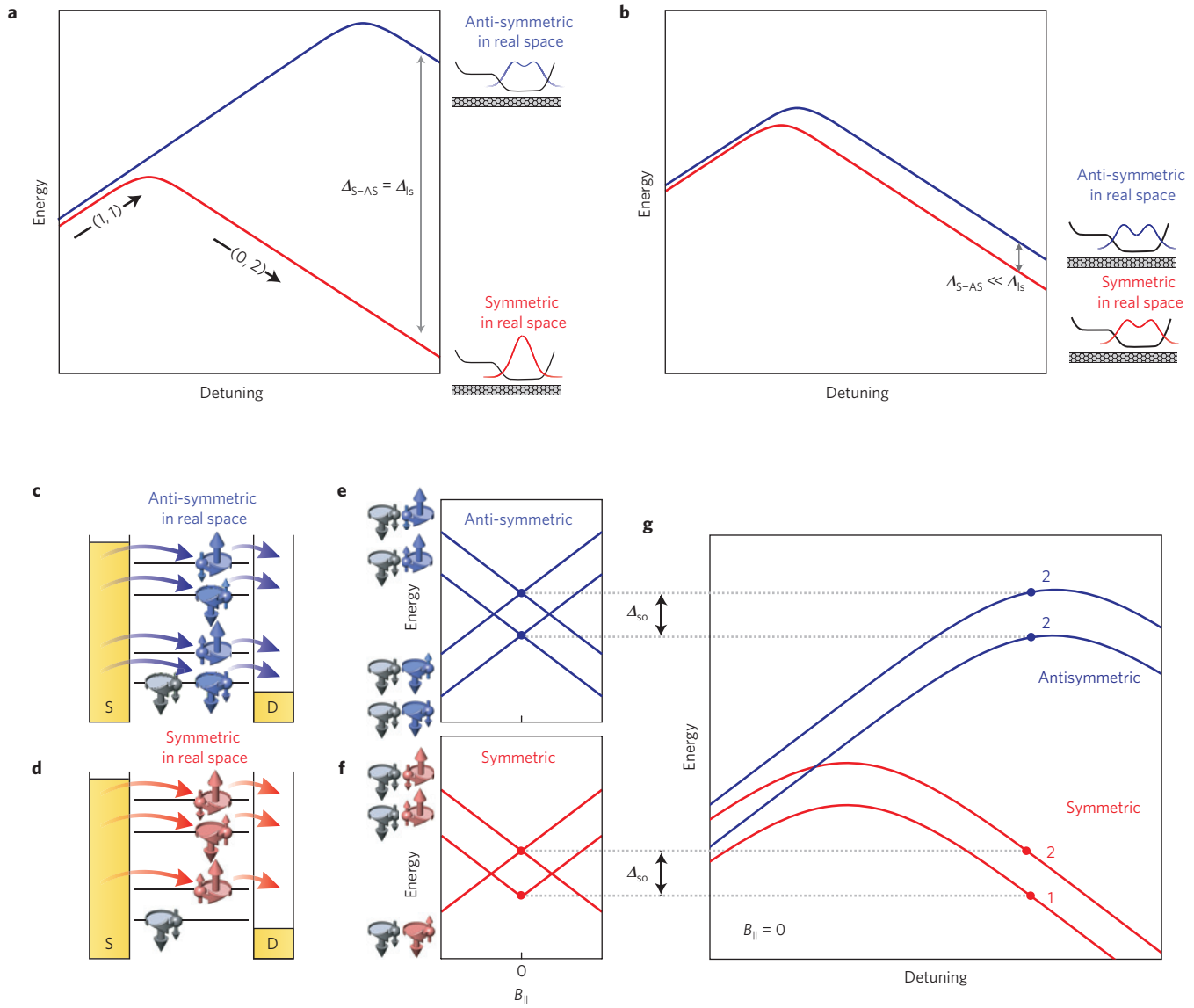

Figure 2 | Addition energy spectra predicted for two non-interacting and two strongly interacting electrons in a nanotube. a, Addition energy of the two lowest 2*e* states as a function of detuning in the non-interacting limit. On the left side the electrons populate the entire nanotube ((1,1) configuration) and on the right they are localized on one side ((0,2) configuration). Colours correspond to the symmetry of 2*e* states in real space (see labels). On the (0,2) side the splitting of these states, Δ_{S-AS}, is equal to the single-particle level spacing, Δ_{ls}. Side insets: charge density profiles calculated for the 2*e* states in the (0,2) configuration. **b**, The same as in **a**, but for the strongly interacting (Wigner molecule) limit. **c**, Spin–isospin states contributing to the transport around the 1*e* to 2*e* Coulomb blockade transition, for a spatially anti-symmetric 2*e* state. The grey symbol is the starting 1*e* state and the blue symbols are the possible states for the added electron. Spin and isospin are denoted by the thin and thick arrows. **d**, The same as in **c**, but for spatially symmetric 2*e* states. **e**, Addition energies of the spatially anti-symmetric 2*e* multiplet as a function of magnetic field parallel to the tube axis, $B_{\parallel}$. The resulting magnetic fingerprint features a double-cross pattern, split at $B_{\parallel} = 0$ by the spin-orbit coupling, Δ_{so}. **f**, The same as for **e**, but for the symmetric multiplet. In this case a characteristic cusp is visible at $B_{\parallel} = 0$. **g**, The expected spectrum of 2*e* states in a nanotube at $B_{\parallel} = 0$, which should be similar either to that in **a** or to that in **b**, depending on the strength of interactions, but should also have two copies of each line due to the spin–isospin degrees of freedom. Numbers above the lines denote their $B_{\parallel} = 0$ degeneracy.

are four possible spin–isospin combinations, whose degeneracy is broken by spin–orbit interactions[13]. Correspondingly, states of two electrons have $4 \times 4 = 16$ possible spin–isospin combinations, 6 of them are spatially symmetric and 10 are spatially anti-symmetric (Supplementary Section S1). Thus, each line in the schematic diagrams of Fig. 2a,b should appear in multiple copies. However, only some copies should be visible in transport experiments that probe 1*e*–2*e* transitions, as illustrated in Fig. 2c,d. In all cases the system starts with one electron in the lowest single-particle state (grey symbol) and a second electron hops in and out, providing a conductance signal. When the two electrons form a symmetric state in real space they cannot occupy the same spin–isospin state (Supplementary Section S1), leaving only the three high-lying states for the added electron (Fig. 2d). When they form an antisymmetric state in real space all four states are available (Fig. 2c). Thus, in total, seven out of the sixteen 2*e* states should appear in transport.

A clear way to experimentally distinguish the symmetric and antisymmetric multiplets is by their magnetic-field fingerprints. A magnetic field parallel to the tube axis, $B_{\parallel}$, couples to both the orbital and spin magnetic moments of the electron (up and down arrows in Fig. 2e–f) and shifts the energy of each spin–isospin state with a unique slope. As was previously demonstrated[13], for a single

© 2013 Macmillan Publishers Limited. All rights reserved

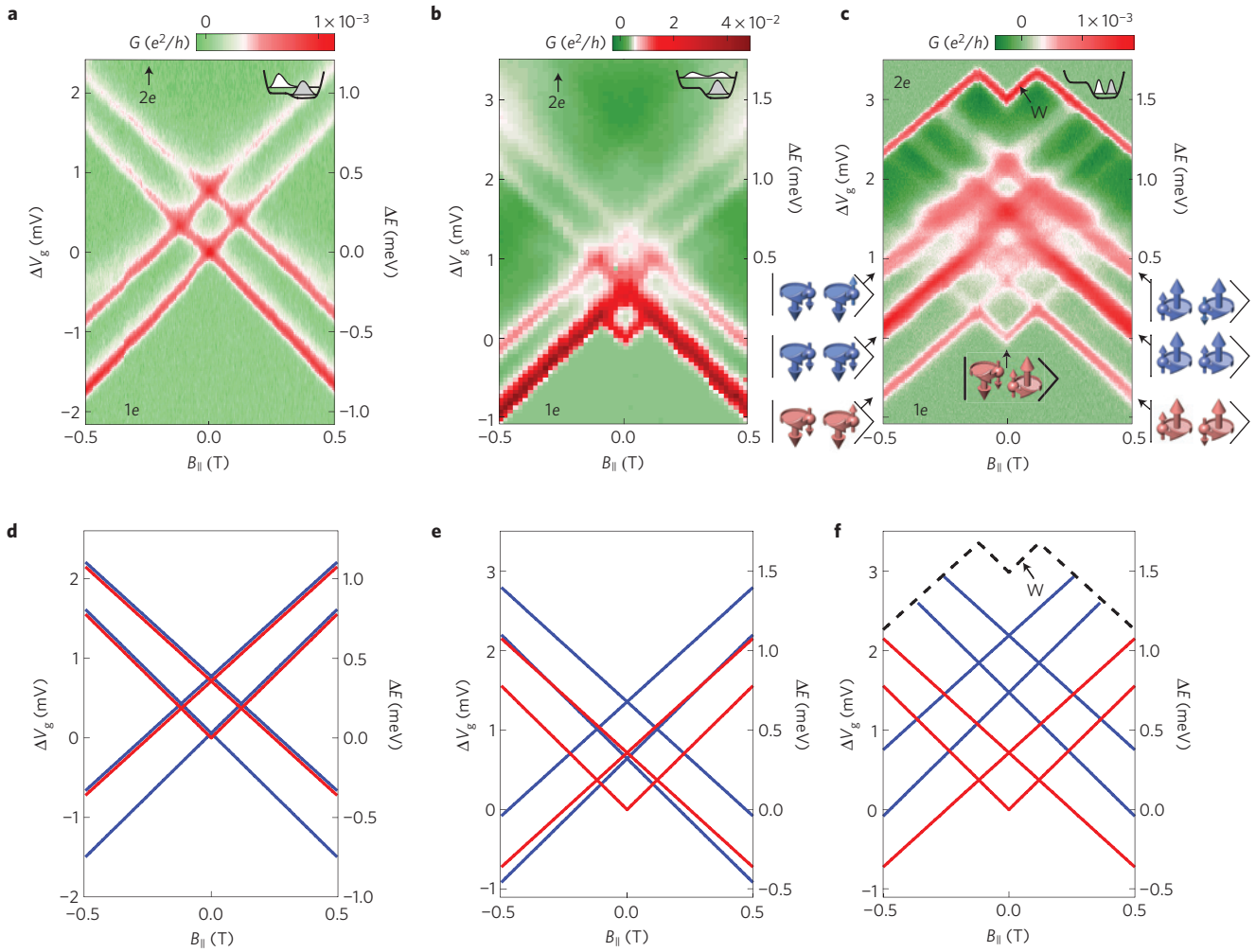

Figure 3 | Magnetic-dependent spectra of the two-electron molecular states at different detunings. a–c, G measured as a function of $B_{\parallel}$ and V_g around the 1e to 2e transition. Lines of enhanced conductance correspond to tunnelling through 2e states. **a** is measured in the (1,1) configuration ($\epsilon = 35$ mV, $V_{sd} = 2$ mV), **c** is in the (0,2) configuration ($\epsilon = 83$ mV, $V_{sd} = -1.7$ mV) and **b** corresponds to a detuning in between these configurations ($\epsilon = 65$ mV, $V_{sd} = -7$ mV). For example, the vertical sweep at $B_{\parallel} = 0$ in **c** corresponds to a horizontal cut at $V_{sd} = -1.7$ mV in Fig. 1d. The line labelled W in **c** corresponds to the similarly labelled line in Fig. 1d, representing the edge of the spectroscopic measurement window. Gate voltage is converted to relative energy (right axis) by $\Delta E = e\Delta V_g(V_{sd}/\Delta W)$, where ΔW is the difference in gate voltage between the ground state and the W line (seen only in **c**). In **c** we use the symbols from Fig. 2e,f to specify the spin and isospin content of each 2e state. **d–f**, Theoretically calculated addition energies as a function of magnetic field for the detunings in **a–c**. Energies of the spatially symmetric states (red) and spatially anti-symmetric states (blue) are calculated with the measured spin and orbital magnetic moments. The splitting between the symmetric and antisymmetric multiplets in each panel is chosen to fit the measurement.

electron this results in a characteristic double-cross structure, split at $B_{\parallel} = 0$ by spin–orbit coupling, Δ_{so}. For two electrons in the non-interacting framework the addition spectrum measured by transport amounts to the energy of the added electron, resulting again in simple fingerprints: in the $2e$ antisymmetric multiplet the added electron can populate all four spin–isospin states and thus the corresponding addition energies will have a double-cross pattern (Fig. 2e) identical to that of a single electron. In the $2e$ symmetric multiplet the lowest state is forbidden, leading to a double-cross without the lowest line (Fig. 2f), having a distinctive cusp at $B_{\parallel} = 0$. We note that the isospin degree of freedom, associated with the motion around the nanotube circumference, involves large energy scales (subband splitting) and is therefore hardly affected by interactions. Thus, the magnetic dependence of the multiplets, derived above in the non-interacting framework, remains a good description also in the presence of interactions. In contrast, the energy scale of the longitudinal degree of freedom is relatively small, and hence the splitting between the multiplets is sensitive to interactions. Depending on the strength of interactions, the multiplets should evolve as a function of detuning, either as the non-interacting case (Fig. 2a) or as the strongly interacting case (Fig. 2b), only that now even at $B_{\parallel} = 0$ we should see two copies of each line, split by Δ_{so} (Fig. 2g). Using the above identification tools we can proceed to experimentally study the $2e$ states. We start by measuring their dependence on $B_{\parallel}$ at three different detunings: in the (1,1) configuration (Fig. 3a), the (0,2) configuration (Fig. 3c) and at the crossover between them (Fig. 3b). In all figures we plot the differential conductance, measured at a finite V_{sd}, as a function of $B_{\parallel}$ and V_g (converted to energy on the right axis). Each line of enhanced conductance arises from a $2e$ state, giving directly the magnetic-field dependence of the $2e$ addition spectrum. Looking first at the (1,1) configuration (Fig. 3a) we identify four lines, two with positive slopes and two with negative slopes. Notably, the magnetic moments and the zero-field splitting (0.34 ± 0.01 meV at $B_{\parallel} = 0$) in this $2e$ spectrum are identical to those in the one-electron double-cross spectrum we reported earlier[13], showing that the

© 2013 Macmillan Publishers Limited. All rights reserved

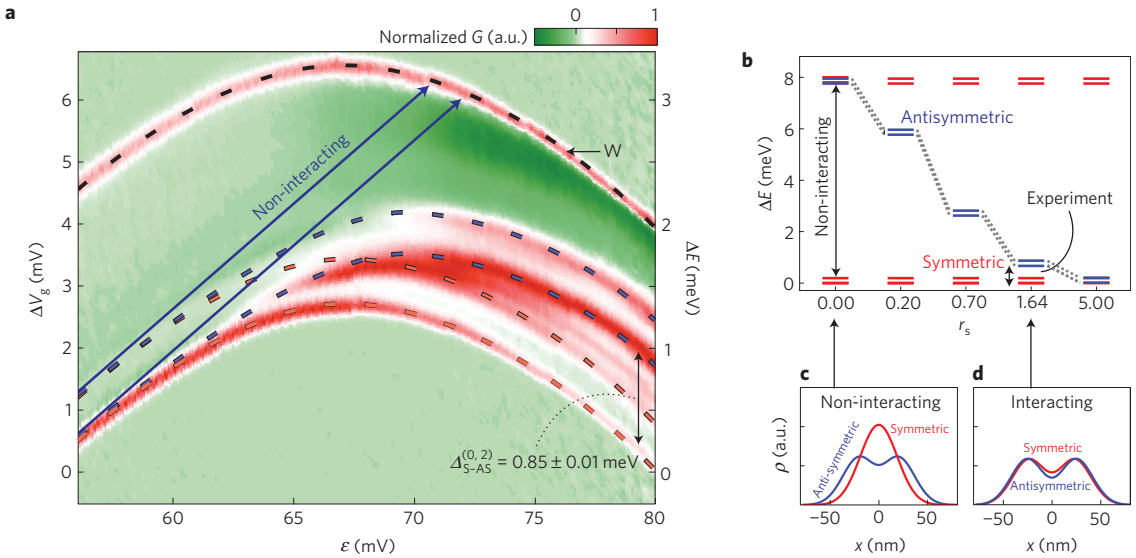

Figure 4 | Quenching of excitation energies in a Wigner molecule. a, G measured as a function of V_g and ϵ at $B_\parallel = 0$ and $V_{sd} = -2$ mV, giving the detuning dependence of the nanotube $2e$ states. To enhance the visibility of individual states we plot the G normalized by its maximal value for every ϵ. Dashed lines are guidelines marking the position of the antisymmetric states (blue) and symmetric states (red), based also on a measurement at an opposite bias (Supplementary Fig. S6). Solid lines indicate the non-interacting prediction for the energy of the antisymmetric states (see Fig. 2a). $\Delta_{S-AS}^{(0,2)}$ labels the splitting between the symmetric and antisymmetric multiplets at large detuning (accurately extracted from Fig. 3c). The W-labelled line gives the edge of the spectroscopic window. **b**, Exact diagonalization calculation of the excitation energies of the symmetric multiplet (red) and antisymmetric multiplet (blue) in the (0,2) charge configuration as a function of interaction parameter r_s. An arrow marks the spectrum that best fits the experimental data ($r_s = 1.64$). States that do not appear in transport are omitted. **c**, Exact diagonalization calculation of the charge density as a function of position along the tube x, $\rho(x)$, in the ground state of the symmetric (red) and antisymmetric (blue) multiplets for $r_s = 0$. **d**, The same as for **c**, but for $r_s = 1.64$.

observed splitting is due to spin–orbit coupling (Supplementary Fig. S3). This allows us to clearly identify the spin and isospin quantum numbers of each state. At higher detuning (Fig. 3b) we observe additional states, most apparent as a cusp at $B_\parallel = 0$. Finally, at even higher detuning in the (0, 2) configuration (Fig. 3c), the double-cross (visible at ∼1 meV above the ground state) remains the strongest feature, while the additional multiplet with a zero-field cusp fully emerges at low energies.

The measured magnetic fingerprints (Fig. 3a–c) show remarkable similarity to the predicted ones (Fig. 3d–f) based on the non-interacting theory (Fig. 2e–f). The low-energy, cusped multiplet observed at high detuning (Fig. 3c) can thus be identified with the symmetric multiplet (red lines, Fig. 3f), and the double-cross at higher energies with the antisymmetric multiplet (blue lines, Fig. 3f). Experimentally, we observe one additional cross between the multiplets (Fig. 3c, at ∼0.6 meV above the ground state), which we associate with inter-valley backscattering processes (Supplementary Section S4). However, apart from it, the non-interacting framework quantitatively describes the entire structure within each multiplet. With decreasing detuning, the splitting between the multiplets decreases (Fig. 3b), until they fully overlap in the (1, 1) configuration (Fig. 3a). We observe a spectrum identical in all of the above details for two holes (Supplementary Fig. S5), demonstrating that all of these observations are generic.

The crucial role played by interactions is unravelled when we measure the detuning dependence of the addition spectrum (Fig. 4a). This figure plots the conductance at $B_\parallel = 0$ as a function of ϵ and V_g (converted to energy on the right axis). The lowest line corresponds to the $2e$ ground state. A parallel line, at energy eV_{sd} above it (labelled W), arises from the width of our spectroscopic window set by $V_{sd} = -2$ mV. The lines in between correspond to excited $2e$ states. These lines are visible in this figure mostly at high detuning due to asymmetric coupling to the leads, whereas measurements at opposite V_{sd} (Supplementary Fig. S6) reveal their complementary dependence at low detuning, and the dashed guiding lines fit the data from both. By associating each state with its magnetic fingerprint in Fig. 3 we identify the pair of symmetric lines (red dashed), the pair of antisymmetric lines (blue dashed) and the single line in between (due to inter-valley backscattering, Supplementary Section S4). Notably all of the lines evolve from an up-going slope at low detuning to a down-going slope at high detuning, clearly indicating that all of them completely evolve from the (1, 1) to the (0, 2) configuration. The spectrum measured at high detuning shown in Fig. 3c is thus a direct observation of the addition spectrum of two electrons in a single dot (similarly for two holes in Supplementary Fig. S5). As explained above, in the absence of interactions, the splitting between symmetric and antisymmetric states should amount to the single-particle level spacing, Δ_{ls}. In Supplementary Section S2 we directly extract this single-particle spacing from measurements of the $1e$ addition spectrum to be $\Delta_{ls} = 7.8 \pm 0.1$ meV and show that the confining potential of one electron approximates well that of two electrons. Remarkably, if we compare this spacing with the symmetric to antisymmetric splitting in the $2e$ spectra we see that this $2e$ excitation energy is quenched by almost an order of magnitude compared with its non-interacting value.

The pronounced quenching of the symmetric–antisymmetric excitation energy as compared with the non-interacting picture attests to the effect of strong electron–electron interactions. To better understand the role of interactions we performed an exact-diagonalization calculation[31] of the excitation spectrum (Supplementary Section S7) corresponding to the parameters of our $2e$ dot, as a function of the dimensionless interaction strength $r_s = d/a_B^*$, where a_B^* is the effective Bohr radius and d is the length scale of the harmonic oscillator potential. Without interactions ($r_s = 0$) the ground state is of the symmetric multiplet, and the antisymmetric multiplet is higher in energy by $\Delta_{ls} = 7.8$ meV. With increasing r_s, the antisymmetric states drop in energy, becoming degenerate with the symmetric states for large r_s. In this limit the two electrons form a Wigner molecule, the transition to this state being continuous owing to the one-dimensionality and small number of electrons.

© 2013 Macmillan Publishers Limited. All rights reserved

Our experimental observation of a tenfold quenching corresponds to the $r_s = 1.64$ case (arrow, Fig. 4b). As explained above, the quenching follows from the spatial separation of the two electrons. This becomes apparent by comparing the calculated electronic charge-density profiles along the nanotube in both multiplets for the non-interacting (Fig. 4c) and interacting (Fig. 4d) cases. Indeed, the density profiles calculated for the observed quenching are nearly identical for the two multiplets, demonstrating the strongly interacting nature of this two-electron Wigner molecule.

In summary, using transport spectroscopy of ultraclean nanotube quantum dots we measure directly the addition spectrum of two interacting electrons or holes. By tuning the one-dimensional confinement potential we go between a state where the electrons are artificially separated by the confining potential to one where their separation is determined solely by their interactions. In the latter case we observe seven quantum states, grouped into two multiplets according to spin–isospin symmetry. The magnetic fingerprint within each multiplet is reproduced by the non-interacting picture. Remarkably, however, the fundamental excitation involving a change in symmetry is markedly quenched in energy compared with its non-interacting value. Using exact-diagonalization calculations we demonstrate that such quenching is a fundamental signature of a strongly interacting Wigner molecule, in which electrons are spatially separated by their mutual repulsion. The spectroscopy of the nanotube Wigner molecule, provided here for the first time, directly shows that suspended carbon nanotubes can host strongly interacting ground states and opens the way for studies of a wider variety of strongly interacting multi-electron states predicted to exist in one-dimensional systems.

Methods

Devices were fabricated from degenerately doped silicon-on-insulator wafers, with a 1.5-μm-thick device layer on top of a 2-μm buried oxide. Using dry etching and thermal oxidation (thickness 100 nm) we isolated two electrically independent mesas from the device layer that served as bottom gates to the nanotube. Gate contacts (2/50 nm Ti/Pt), source and drain electrodes (5/25 nm Cr/Pt) and catalyst pads were patterned using electron-beam lithography. Nanotubes were grown after completing all patterning to produce clean devices. All measurements were performed in a dilution refrigerator with a base temperature of $T = 30$ mK. The electron temperature extracted from the width of the Coulomb peaks was 100–200 mK. The conductance was measured using standard lock-in techniques with small excitations (typically 4–10 μV).

Received 31 January 2013; accepted 10 June 2013; published online 28 July 2013

References

1. Bryant, G. Electronic structure of ultrasmall quantum-well boxes. *Phys. Rev. Lett.* **59,** 1140–1143 (1987).
2. Häusler, W. & Kramer, B. Interacting electrons in a one-dimensional quantum dot. *Phys. Rev. B* **47,** 16353–16357 (1993).
3. Meyer, J. S. & Matveev, K. A. Wigner crystal physics in quantum wires. *J. Phys. Condens. Matter* **21,** 023203 (2009).
4. Egger, R. & Gogolin, A. Effective low-energy theory for correlated carbon nanotubes. *Phys. Rev. Lett.* **79,** 5082–5085 (1997).
5. Kane, C., Balents, L. & Fisher, M. Coulomb interactions and mesoscopic effects in carbon nanotubes. *Phys. Rev. Lett.* **79,** 5086–5089 (1997).
6. Bockrath, M. *et al.* Luttinger-liquid behaviour in carbon nanotubes. *Nature* **397,** 598–601 (1999).
7. Yao, Z., Postma, H. W. C., Balents, L. & Dekker, C. Carbon nanotube intramolecular junctions. *Nature* **402,** 540–544 (1999).
8. Ishii, H. *et al.* Direct observation of Tomonaga–Luttinger-liquid state in carbon nanotubes at low temperatures. *Nature* **426,** 540–544 (2003).
9. Jarillo-Herrero, P., Sapmaz, S., Dekker, C., Kouwenhoven, L. P. & Van Der Zant, H. S. J. Electron-hole symmetry in a semiconducting carbon nanotube quantum dot. *Nature* **429,** 389–392 (2004).
10. Minot, E. D., Yaish, Y., Sazonova, V. & McEuen, P. L. Determination of electron orbital magnetic moments in carbon nanotubes. *Nature* **428,** 536–539 (2004).
11. Cao, J., Wang, Q. & Dai, H. Electron transport in very clean, as-grown suspended carbon nanotubes. *Nature Mater.* **4,** 745–749 (2005).
12. Deshpande, V. V. & Bockrath, M. The one-dimensional Wigner crystal in carbon nanotubes. *Nature Phys.* **4,** 314–318 (2008).
13. Kuemmeth, F., Ilani, S., Ralph, D. C. & McEuen, P. L. Coupling of spin and orbital motion of electrons in carbon nanotubes. *Nature* **452,** 448–452 (2008).
14. Steele, G. A., Gotz, G. & Kouwenhoven, L. P. Tunable few-electron double quantum dots and Klein tunnelling in ultraclean carbon nanotubes. *Nature Nanotechnol.* **4,** 363–367 (2009).
15. Ellenberger, C. *et al.* Excitation spectrum of two correlated electrons in a lateral quantum dot with negligible Zeeman splitting. *Phys. Rev. Lett.* **96,** 126806 (2006).
16. Kalliakos, S. *et al.* A molecular state of correlated electrons in a quantum dot. *Nature Phys.* **4,** 467–471 (2008).
17. Singha, A. *et al.* Correlated electrons in optically tunable quantum dots: Building an electron dimer molecule. *Phys. Rev. Lett.* **104,** 246802 (2010).
18. Kristinsdóttir, L. *et al.* Signatures of Wigner localization in epitaxially grown nanowires. *Phys. Rev. B* **83,** 041101(R) (2011).
19. Jespersen, T. S. *et al.* Gate-dependent spin–orbit coupling in multielectron carbon nanotubes. *Nature Phys.* **7,** 348–353 (2011).
20. Pei, F., Laird, E. A., Steele, G. A. & Kouwenhoven, L. P. Valley-spin blockade and spin resonance in carbon nanotubes. *Nature Nanotechnol.* **7,** 630–634 (2012).
21. Secchi, A. & Rontani, M. Coulomb versus spin–orbit interaction in few-electron carbon-nanotube quantum dots. *Phys. Rev. B* **80,** 041404(R) (2009).
22. Wunsch, B. Few-electron physics in a nanotube quantum dot with spin–orbit coupling. *Phys. Rev. B* **79,** 235408 (2009).
23. Pályi, A. & Burkard, G. Spin-valley blockade in carbon nanotube double quantum dots. *Phys. Rev. B* **82,** 155424 (2010).
24. Secchi, A. & Rontani, M. Wigner molecules in carbon-nanotube quantum dots. *Phys. Rev. B* **82,** 035417 (2010).
25. Von Stecher, J., Wunsch, B., Lukin, M., Demler, E. & Rey, A. M. Double quantum dots in carbon nanotubes. *Phys. Rev. B* **82,** 125437 (2010).
26. Kuemmeth, F., Churchill, H. O. H., Herring, P. K. & Marcus, C. M. Carbon nanotubes for coherent spintronics. *Mater. Today* **13,** 18–26 (March, 2010).
27. Ingerslev Jørgensen, H. *et al.* Singlet–triplet physics and shell filling in carbon nanotube double quantum dots. *Nature Phys.* **4,** 536–539 (2008).
28. Churchill, H. O. H. *et al.* Relaxation and dephasing in a two-electron 13C nanotube double quantum dot. *Phys. Rev. Lett.* **102,** 166802 (2009).
29. Churchill, H. O. H. *et al.* Electron–nuclear interaction in 13C nanotube double quantum dots. *Nature Phys.* **5,** 321–326 (2009).
30. Laird, E., Pei, F. & Kouwenhoven, L. A valley-spin qubit in a carbon nanotube. Preprint at http://arxiv.org/abs/1210.3085 (2012).
31. Rontani, M., Cavazzoni, C., Bellucci, D. & Goldoni, G. Full configuration interaction approach to the few-electron problem in artificial atoms. *J. Chem. Phys.* **124,** 124102 (2006).

Acknowledgements

We would like to acknowledge E. Berg, A. Stern, A. Yacoby and B. Wunsch for useful discussions. S.I. acknowledges the financial support by the ISF Legacy Heritage foundation (2005/08-80.0), the Bi-National science foundation (BSF 710647-03), the Minerva foundation, the ERC starters grant (258753), the Marie Curie People grant (IRG 239322), and the Alon fellowship. S.I. is incumbent of the William Z. and Eda Bess Novick career development chair. P.L.M. and D.C.R. acknowledge support by the NSF through the Center for Nanoscale systems (EEC-0646547), by the NSF through DMR-1010768, and by the MARCO Focused Research Center on Materials, Structures and Devices. The experiments used the facilities of the Cornell node of the National Nanotechnology Infrastructure Network (EECS-0335765) and the Cornell Center for Materials Research (DMR-1120296), both funded by NSF. M.R. and A.S. acknowledge support from Fondazione Cassa di Risparmio di Modena through the project COLD and FEW, from EU through the Marie Curie ITN INDEX, and from the CINECA-ISCRA supercomputing grant IscrC_TUN1DFEW. F.K. acknowledges support by the Center for Quantum Devices, funded by the Danish National Research Foundation.

Author contributions

F.K., S.I., D.C.R. and P.L.M. conceived and designed the experiments. F.K. and S.I. performed the experiments. S.P., A.S. and M.R. provided theoretical tools for analysing the data. S.P., F.K., A.S., M.R. and S.I. analysed the data. S.P. and S.I. wrote the manuscript and all authors contributed to its final version.

Additional information

Supplementary information is available in the online version of the paper. Reprints and permissions information is available online at www.nature.com/reprints. Correspondence and requests for materials should be addressed to S.I.

Competing financial interests

The authors declare no competing financial interests.

© 2013 Macmillan Publishers Limited. All rights reserved